International Journal of Shape Modeling,

FAITHFUL RECOVERING OF QUADRIC SURFACES FROM 3D RANGE DATA BY GLOBAL FITTING

NAOUFEL WERGHI* , BOB FISHER, ANTHONY ASHBROOK*, CRAIG ROBERTSON
Division of Informatics, University of Edinburgh, 5 Forrest Hill
Edinburgh, Scotland, United Kingdom

The paper proposes a reliable method for estimating quadric surfaces from 3D range data in the framework of object recognition and localization or reverse engineering. Instead of estimating a quadric surface in isolation, the approach fits all the surfaces captured in the scene together taking into account the geometric relationships between them and their specific characteristics. The technique is compared with other methods through experiments performed on real objects and demonstrates that the use of constrained relationships improves shape estimates.

Keywords: Quadric surfaces, surface fitting, non-linear optimization, shape modelling.

1. Introduction

Common quadric surfaces such as cylinders, cones and spheres are found in most manufactured parts and objects. A reliable estimation of these surfaces is a fundamental requirement in many applications. An example is in the framework of model-based recognition and localization of objects from range data, where the parameters of the surfaces are used for detecting plausible correspondences between model and scene or between surfaces extracted from different views for registration purposes. An accurate and reliable estimation of surfaces is also an essential requirement in object modelling or reverse engineering, where a faithful model is needed to be extracted from the set of range data for CAD/CAM purposes.

One obstacle to achieving this goal is the inaccuracy of shape estimates from extracted quadric patches. This problem results from the limited field of view of the sensor which can only cover a partial area of an object in a given view, self or external occlusion of the object and finally some surface data is lost during the surface segmentation process either due to segmentation failure or intentionally in order to avoid unreliable data. The usable set of data points may thus represent only a small area of the surface (Figure 1) and consequently give unstable estimates of the surface shape. Furthermore the available data is corrupted by measurement noise. Consequently quadric surface fitting often fails to give a reliable estimate of the surface shape. The estimates are highly biased and may not reflect the actual type of the surface even when sophisticated techniques are applied.

The idea presented here is to compensate the poorness of information embodied in the quadric surface data by extra knowledge about the surface such as its type

*Now at the Department of Computing Science, University of Glasgow, Glasgow G12 8QC, UK

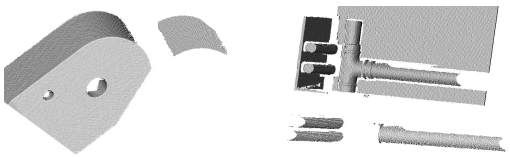

(a) (b)

Figure 1: (a) Object containing a cylindrical surface. Only a small area of of the cylinder surface is visible. (b) A miniaturized model of an industrial plant. Because of noise and segmentation errors only small portions of the pipes are extracted and can be used reliably for shape estimation.

and relationships with other nearby surfaces. This additional information is either provided by the model in the case of model-based applications or deduced from a set of potential hypotheses generated, checked and verified within a perceptual organization process. E.g., if preliminary estimates of a cylinder and plane lead to an angle between the plane normal and the cylinder axis close to 0^o, it is very likely that the two surfaces are orthogonal, or if the estimated shape of a quadric is an elliptic cylinder with major and minor axes having nearly identical values, then it is very likely that the cylinder is circular.

The exploitation of this extra information is quite feasible since a patch is rarely captured alone in the scene but rather with close or adjacent surfaces which could be either planes or quadrics.

This paper shows how the extra information can be represented in a shape estimation process and then evaluates the estimation process against several alternatives, concluding that the extra information is both effective and easy to exploit.

2. Problem statement and related work

A quadric surface S is represented by the implicit function:

$$f(x,y,z,\vec{p}) = ax^2 + by^2 + cz^2 + 2hxy + 2gxz + 2fyz + 2ux + 2vy + 2wz + d = 0 \quad (1)$$

Given a set of N measurement points X_i we want to find the parameter vector $\vec{p} = [a,b,c,h,g,f,u,v,w,d]$ such that the function defined by (1) represents as well as possible the actual shape of the surface. The type and shape characteristics of the surface are deduced afterwards from $\vec{p}$.

A reasonable criterion to judge the goodness of the solution is the sum of the squared Euclidean distances between each measurement point and the surface $J = \sum_{i=1}^{N} d(X_i, S)^2$. The parameter vector minimizing this criterion is the best solution in the least squares sense. Unfortunately the non-linearity of this distance measure does not lead to an easy closed-form solution. Various approximations of this distance have been therefore proposed in the literature to make the minimization problem easier. The most common one is using the value of the implicit function $f(x,y,z)$ known as the algebraic distance. It has been used in recovering

planes and quadrics [1, 2]. Although this approximation is highly attractive because of its closed-form solution, it is subject to much criticism since it leads to a highly biased estimation for small surfaces with low curvature. An improved approximation was suggested by expanding the implicit function by a Taylor's series up to first or second degree. The first order approximation is given by:

$$\frac{|f(x,y,z)|}{\|\vec{\nabla} f(x,y,z)\|} \tag{2}$$

Taubin [3] noted that, for surfaces with constant gradient, the estimate based on the first order approximation is the solution of a generalized eigenvalue problem:

$$H\vec{p} = \lambda DH\vec{p} \tag{3}$$

where $H = \sum_i \vec{h_i}\vec{h_i}^T$, $DH = \sum_i dh_i dh_i^T$,
$\vec{h_i} = [x_i^2, y_i^2, z_i^2, 2x_iy_i, 2x_iz_i, 2y_iz_i, 2x_i, 2y_i, 2z_i, 1]^T$ and dh_i is the Jacobian matrix of $\vec{h_i}$ with respect to $[x_i, y_i, z_i]$. Other than this case the problem is a non-linear minimization which needs to be solved iteratively, e.g. the algorithm proposed by Kumar *et al* [4] for fitting Hyperquadric surfaces. When the gradient of the surface vanishes, the first approximation is no longer valid. To avoid this singularity problem Taubin [5] introduces a higher order approximate distance and estimates the solution with a non-linear fitting procedure. Lukács *et al* [6] tackled this problem by considering an approximation of the geometric distance specific to each quadric type.

Lei and Cooper [7] used both the first and second order approximation for fitting 2D curves but they convert the minimization problem to linear programming optimization by using the measurements points as control points constraining the shape of the curve. Sullivan *et al* [8] minimized the sum of the exact geometric distances and consider the implicit function representing the surface as a constraint function. They solved the problem with an iterative algorithm using the Levenberg-Marquardt technique and Newton method.

Another way for considering the Euclidean distance is to use a specific representation function for a particular case of quadric surfaces, like the circular cylinder, circular cone and sphere. A circular cylinder can be defined by:

$$(x-x_o)^2+(y-y_o)^2+(z-z_o)^2-(n_x(x-x_o)+n_y(y-y_o)+n_z(z-z_o))^2-r^2 = 0 \tag{4}$$

where $\vec{X_o} = [x_o, y_o, z_o]^T$ is an arbitrary point on the axis, $\vec{n} = [n_x, n_y, n_z]^T$ is a unit vector along the axis and r is the radius of the cylinder.

A circular cone can be represented by:

$$[(x-x_o)^2+(y-y_o)^2+(z-z_o)^2]cos^2(\alpha)-[n_x(x-x_o)+n_y(y-y_o)+n_z(z-z_o)]^2 = 0 \tag{5}$$

where $[x_o, y_o, z_o]^T$ is the apex of the cone, $[n_x, n_y, n_z]^T$ is the unit vector defining the orientation of the cone axis and α is the semi-vertical angle.

A sphere can be defined by:

$$(x - x_o)^2 + (y - y_o)^2 + (z - z_o)^2 - r^2 = 0 \tag{6}$$

where $[x_o, y_o, z_o]^T$ is the centre of the sphere and r is its radius.

With this representation the value of the error function at a given point is the squared distance between this point and the surface. This representation and a slightly different one (replacing the axis vector by two angles) were used respectively in [9, 10]. In both works the solution was found with a non-linear optimization.

A common characteristic of these works is that they treated each single surface individually. When the quadric patch to be fitted covers a small amount of the surface, the fitting technique fails to give a reasonable estimate and often the estimates are highly biased. This is expected since second order functions can easily trade-off curvature and position to produce similar error measures. Thus small patches do not provide sufficient extent to reliably select both the curvature and position.

However, if we place ourselves in an object recognition and localization framework, we usually have to estimate many surfaces belonging to the same object that are linked by geometrical and topological relationships. By exploiting this global knowledge together with information that may be available about the quadric type and shape we compensate for the lack of information in the quadric patch and obtain therefore a more accurate surface parameter estimate.

We will show that by a simple representation of the extra information and with a rigorous integration of this information in the fitting process and by using just the algebraic distance, the proposed approach makes a good trade-off between estimation accuracy and computational cost.

3. Principle of the approach

Consider a set of M surface patches of an object extracted from a given view. We assume that the set may contain quadric and planar patches. By considering the algebraic distance the minimization criterion related to the surface k has the form: $J_k = \sum_{i=1}^{N_k} f(x_i, y_i, z_i, \vec{p_k})^2$ for N_k data points $(x_i, y_i, z_i)^T$ lying on the surface. This expression can be put into the form $J_k = \vec{p_k}^T \mathcal{H}_k \vec{p_k}$ where $\vec{p_k}$ is the parameter vector and H_k is a nonnegative, definite and symmetric matrix:

$$H_k = \sum_{i=1}^{N_k} \vec{h_i} \vec{h_i}^T \tag{7}$$

$\vec{h}$ is a measurement vector function of the measurement point $(x, y, z)^T$. E.g. for a plane and a quadric $\vec{h}$ is defined respectively by: $\vec{h} = [x, y, z, 1]^T$ and for a quadric surface $\vec{h} = [x^2, y^2, z^2, 2xy, 2xz, 2yz, 2x, 2y, 2z, 1]^T$. A global minimization criterion for all the surfaces is the sum of all the single criteria

$$J = J_1 + J_2 + \cdots + J_M = \vec{p}^T \mathcal{H} \vec{p} \tag{8}$$

where $\vec{p}$ is a global parameter vector concatenating all the single parameter vectors and $\mathcal{H}$ is a global data matrix containing the set of matrices $\mathcal{H}_k$. $\mathcal{H}$ is nonnegative, definite and symmetric as well. Examples on how the matrix $\mathcal{H}$ is formed in terms of block-matrix $\mathcal{H}_k$ for different objects are shown in Section 5. The relationships between the different surfaces and the shape characteristics of the surfaces are formulated into a set of vector functions

$$C_j(\vec{p}) = 0, \quad j = 1..K \tag{9}$$

So, the problem can be seen as a constrained optimization problem where we have to determine the parameter vector $\vec{p}$ minimizing (8) subject to the constraints (9).

In a previous work [11] concerned with reverse engineering, we developed an algorithm to solve such constrained problems. Very briefly, the algorithm is based on sequential unconstrained programming technique where each constraint is assigned a weighting value. The set of weights are incremented sequentially, and at each iteration the optimisation function composed of the least squares term (8) and the weighted constrained functions (9) is minimized by means of a standard Levenberg-Marquardt Technique. The algorithm stops when the constraints are satisfied to the desired degree or when the parameter vector remains stable for a certain number of iterations. The constraints were represented with the following matrix formulation

$$C(\vec{p}) = (\vec{p}^T A\vec{p} + B^T\vec{p} + V)^2 \tag{10}$$

where A and B are respectively a square matrix and a vector having the same dimension as the parameter vector $\vec{p}$, V is a scalar. For more details about the approach, we recommend the readers to [11].

4. Parametrization of the cylinder, the cone and the sphere

When the treated object contains planes and quadrics the relationships between a quadric surface and other surfaces are relative orientation and position for cylinders and cones and relative position for spheres. The circularity of a cylinder or a cone is additional knowledge about the quadric shape which should be taken into account as well.

Unfortunately the coefficients of the implicit function (1) do not have obvious geometric significance. Formulating the geometric relationships only with these parameters leads to complex constraint functions often with singular cases. To avoid this problem, we introduce the orientation of the quadric axis defined by a normal vector $[n_x, n_y, n_z]^T$ as additional parameters for the cylinder and the cone. Each of these two surfaces will be defined then by the following parameter vector:

$$[a, b, c, h, g, f, u, v, w, d, n_x, n_y, n_z]^T \tag{11}$$

This representation over-parameterizes the quadric; in return it allows a simple formulation of the geometric relationships between cone, cylinder and other surfaces

e.g. the relative orientation between a plane and a quadric is expressed by

$$\vec{n_c}^T \vec{n_p} - cos(\alpha) = 0; \tag{12}$$

where α is the angle between the plane's normal and the quadric axis, $\vec{n_c}$ is the orientation vector of the quadric axis and $\vec{n_p}$ is the plane's normal.

Based on the above parametrization the circularity of the cylinder is expressed by the following equations

$$\begin{aligned} a &= 1 - n_x^2 & \qquad h &= -n_x n_y \\ b &= 1 - n_y^2 & \qquad g &= -n_x n_z \\ c &= 1 - n_z^2 & \qquad f &= -n_y n_z \end{aligned} \tag{13}$$

and for the cone by:

$$\begin{aligned} a - b &= n_x^2 - n_y^2 & \qquad h &= n_x n_y \\ a - c &= n_x^2 - n_z^2 & \qquad g &= n_x n_z \\ b - c &= n_y^2 - n_z^2 & \qquad f &= n_y n_z \end{aligned} \tag{14}$$

These relations are obtained by expanding equations (4) and (5) and identifying with the general quadric equation (1). Taking into account the set of equations (13), we can show that the point defined by $X_o = [-u, -v, -w]^T$ belongs to the cylinder axis, and that the cylinder radius can be expressed by

$$r^2 = d - u^2 - v^2 - w^2 \tag{15}$$

A sphere is characterized by equal coefficients for the x^2, y^2 and z^2 terms and vanishing coefficients for the cross product terms. Its representation is:

$$a(x^2 + y^2 + z^2) + 2ux + 2vy + 2wz + d = 0 \tag{16}$$

The radius and the centre of the sphere are defined respectively by

$$\vec{X_o} = [-u/a, -v/a, -w/a]^T \tag{17}$$

$$r^2 = \frac{u^2 + v^2 + w^2 - ad}{a^2} \tag{18}$$

5. Experiments

A series of experiments were performed on several real objects having planar and quadric surfaces. The segmentation and the extraction of the surfaces were performed automatically with the *rangeseg* program[12].

Our approach was compared with three main techniques covering a large part of the spectrum of the fitting techniques developed in the literature. These techniques are the unconstrained algebraic distance (AD) [1, 2], the first order approximation

of the Euclidean distance (AED) [3] (2) and the iterative optimization technique [9, 10] based on the specific representations (SR) of quadrics (13), (14) and (6), respectively for the circular cone, the circular cylinder and the sphere. We note that the AED technique used here is improved with respect to the one in [3] by weighting the Euclidean distance by the data variances (see the Appendix for details). In the rest of the paper these techniques will be referenced respectively by AD, AED, SR and our proposed global fitting approach by GF.

The performances of the different techniques are evaluated by comparing the shape parameters of the quadrics, for instance the half angle for the cone and the radius for the cylinder and the sphere. The computation time was taken into account as well. With AD, and AED the estimation time is almost instantaneous, whereas it varies from half an hour to several hours for the SR depending on the number of measurement points. For the GF technique it is in the range of minutes. The different techniques were implemented with Matlab on a 200 MHz Sun UltraSparc workstation.

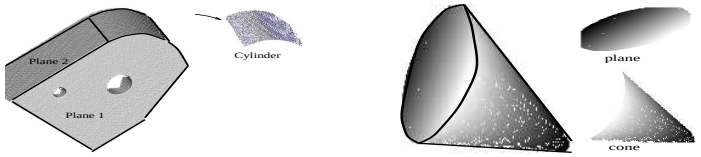

(a) object 1 (b) object 2

Figure 2: Objects used in the experiments with the extracted surfaces. The boundaries of the extracted surfaces are marked on the object.

Consider object 1 containing a cylindrical patch and plane surface patches. In the view shown in Figure 2.(a), only a small part of the cylinder surface is visible (about 20%). The cylinder is circular and its axis is orthogonal to plane 1 and parallel to plane 2. The first constraint is imposed by using a single unit vector for both the cylinder axis and the normal of plane 1. The second constraint is satisfied by imposing

$$\vec{n_1}^T \vec{n_2} = 0 \tag{19}$$

where $\vec{n_1}$ and $\vec{n_2}$ are the normals of plane 1 and plane 2. The parameter vector is then $\vec{p} = [a, b, c, h, g, f, u, v, w, d, n_{1_x}, n_{1_y}, n_{1_z}, l_1, n_{2_x}, n_{2_y}, n_{2_z}, l_2]$ where l_1 and l_2 are the distance parameters of plane 1 and plane 2. The minimization criterion is

$$J = \vec{p}^T \mathcal{H} \vec{p}, \quad \mathcal{H} = \begin{bmatrix} H_{cylinder} & (O) & (O) \\ (O) & H_{plane1} & (O) \\ (O) & (O) & H_{plane2} \end{bmatrix}$$

where $H_{cylinder}$, H_{plane_1} and H_{plane_2} are the data matrices of the cylinder surface, plane 1 and plane 2, computed with (7).

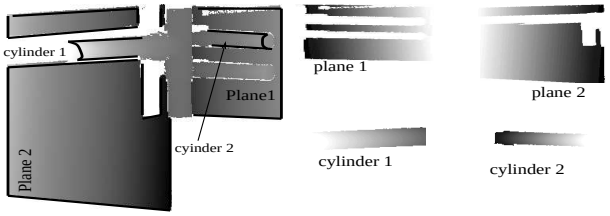

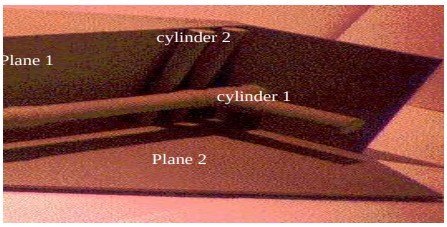

(a) object 3

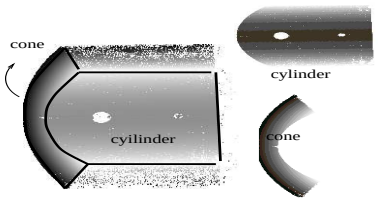

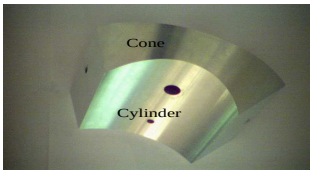

(b) object 4

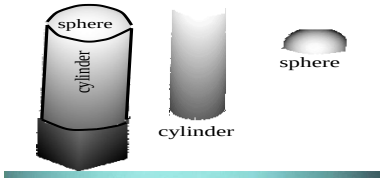

(c) object 5

Figure 3: Objects used in the experiments with the extracted surfaces. The boundaries of the extracted surfaces are marked on the object.

From (19) we deduce the penalty function associated to the orientation constraint: $C_{orient}(\vec{p}) = (\vec{p}^T A \vec{p})^2$ where A is an appropriate matrix.

The penalty function related to the circularity constraint is deduced from (13) and defined by: $C_{circ}(\vec{p}) = \sum_{i=1}^{6} (\vec{u_i}^T \vec{p} - \vec{p}^T L_i \vec{p})^2$

The unity of the normal vectors has to be taken into account as well by introducing the penalty function: $C_{unit}(\vec{p}) = (\vec{p}^T U_1 \vec{p} - 1)^2 + (\vec{p}^T U_2 \vec{p} - 1)^2$ where U_1, U_2 are appropriate matrices.

The optimization function is thus set up as follows:

$$E(\vec{p}) = \vec{p}^T \mathcal{H} \vec{p} + \lambda_{unit} C_{unit}(\vec{p}) + \lambda_{orient} C_{orient}(\vec{p}) + \lambda_{circ} C_{circ}(\vec{p})$$

which can be put into the form $E(\vec{p}) = \vec{p}^T \mathcal{H} \vec{p} + \sum_{k=1}^{9} \lambda_k (C_k(\vec{p}))^2$
where $C_k(\vec{p})$ are the elementary constraint functions in the form of (10).

The results obtained with the different techniques when applied to the objects in Figure 2.a are grouped in Table1.(a). The AD and the AED techniques both give a biased estimates and the resulting estimated cylinder has an elliptical shape. The SR and the GF preserve the circularity of the cylinder surface, the GF has more accurate estimate however. The computation time for the SR technique is 40 min whereas it is only 3 min for the GF technique.

Object 2 is composed of a cone and a plane base (Fig.2.(b)). The axis of the cone is perpendicular to the plane. This constraint is imposed by associating a single unit vector to both the orientation of the cone axis and the plane's normal.

Table1.(b) shows the results obtained with the different techniques except for the AED technique, which cannot be used as a cone surface does not have a constant gradient value. The AD technique gives an elliptic cone, whereas the SR and GF ensures a faithful shape estimate and relatively better accuracy with the GF.

Object 3 is a miniaturized factory model. Two cylinders and two planes were extracted from the view shown in Figure 3.(a). Cylinder 1 and cylinder 2 are orthogonal respectively to plane 1 and plane 2. These constraints are satisfied by associating the same vector to each pair of (Plane1 normal, cylinder 2 orientation) (Plane2 normal, cylinder 1 orientation). The two cylinders are circular and mutually orthogonal. The different estimates are presented in Table 1.(c).

Object 4 (Fig.3.(b)) contains a circular cone and a circular cylinder having perpendicular axes. The cylindrical patch covers nearly 20% of the whole cylinder and the cone patch around 30%. We have not considered the relationships between the two lateral planes and the quadric surfaces but they can be also integrated without any particular difficulty. Since the patches contain a large amount of data points (nearly 25000 and 7000 points for the cylinder and the cone respectively) the SR fitting is quite time-consuming, about six hours for the cylinder and around two hours for the cone. With the GF technique, the two surfaces are simultaneously estimated in 5 min. The different estimates are summarized in Table 1.(d).

Object 5 (Figure 3.(c)) contains a circular cylinder and a half sphere. The two surfaces have the same radius and the axis of the cylinder goes through the centre

of the sphere. In the view shown in Figure 3.(c)) nearly a quarter of the sphere and half of the cylinder are visible. The estimates are shown in Table 1(e).

In terms of accuracy, it is clear that the SR and the GF algorithms are comparable to each other and superior to the AD and the AED algorithms. In terms of speed, GF is an order of magnitude faster.

Figure 4 shows the estimates of the cylinder surface and the sphere surface as we vary the viewpoint on the surface. In the first position (first column) the sphere patch occupies a larger field of the view relatively to the cylindrical patch. Then the object is rotated such that the sphere patch area is reduced and the cylindrical patch becomes more visible in the scene. The sphere patches area ranges from nearly 70% to 20% of a half sphere. We notice that the GF fitting estimates remain stable and close to the actual values. The SR estimates are also relatively stable but less accurate than those of the GF. The AED technique estimates vary dramatically for the cylinder. For the sphere, the AED estimates are relatively stable but still less accurate than the GF ones.

70% sphere patch area 20% (half sphere)

							
cylinder	AED	15.36 15.85	15.16 15.62	11.63 11.68	14.59 14.92	13.91 14.35	14.82 14.90
	SR	15.07	15.05	15.06	15.11	15.11	15.12
	GF	15.04	15.07	14.96	15.03	15.05	15.07
sphere	AED	15.13	15.19	15.16	15.16	15.21	15.24
	SR	15.12	15.18	15.14	15.15	15.19	15.22
	GF	15.04	15.07	14.96	15.03	15.05	15.07

Figure 4: Sphere and cylinder estimates for different positions of object7.

6. Discussion and Conclusion

It is clearly noticed from the different tables related to objects having circular cones or circular cylinders that when the shape of the quadric is not constrained the AD and AED algorithms do not guarantee a faithful shape estimate. Both techniques result in elliptic cones or elliptic cylinders with a bias depending on how much the patch covers the quadric and the number of measurement points in each patch. However the AED technique estimates are less biased. Figure 5 illustrates the difference where the bias in the shape estimates is expressed in terms of the (minor axis/major axis) ratio. The same aspect is noticed for the cones if we compare the cone estimates for object 1 (Table 1.(a)) and object 6 (Table 1(d)).

By imposing the circularity constraint the SR and the GF give faithful estimates in terms of shape and parameter values. It is noticed however that the results are usually more accurate with the GF. This suggests that, by taking into account the different position and orientation relationships constraining the location of the

AD	AED	SR	GF	true surface
ell.cylinder $r_{max} = 30.41$ $r_{min} = 17.50$	ell.cylinder $r_{max} = 41.58$ $r_{min} = 37.80$	cir.cylinder $r = 44.25$	cir.cylinder $r = 44.62$	cir.cylinder $r = 45$
-	-	40 min	3 min	

(a) cylinder in Figure 2.a

AD	AED	SR	GF	true surface
ell.cone: $\alpha_{max} = 21.41^o$ $\alpha_{min} = 20.19^o$	- - -	cir.cone $\alpha = 20.77^o$	cir.cone $\alpha = 19.68^o$	cir.cone $\alpha = 20^o$
-	-	30 min	2 min	

(b) cone in Figure 2.b

AD	AED	SR	GF	true surface
ell.cylinder $r1_{max} = 17.69$ $r1_{min} = 12.12$ $r2_{max} = 4.96$ $r2_{min} = 4.28$	ell.cylinder $r1_{max} = 9.01$ $r1_{min} = 8.13$ $r2_{max} = 5.67$ $r2_{min} = 5.24$	cir.cylinder $r1 = 8.08$ $r2 = 5.23$	cir.cylinder $r1 = 7.44$ $r2 = 4.95$	cir.cylinder $r1 = 7.50$ $r2 = 5.00$
-	-	30 min	5min	

(c) cylinders 1 and 2 in Figure 3.a

AD	AED	SR	GF	true surface
ell.cylinder $r_{max} = 46.10$ $r_{min} = 33.66$	ell.cylinder $r_{max} = 57.62$ $r_{min} = 55.42$	cir.cylinder $r = 59.81$	cir.cylinder $r = 59.54$	cir.cylinder $r1 = 60$
ell.cone $\alpha_{max} = 28.86^o$ $\alpha_{min} = 25.19^o$	- - -	cir.cone $\alpha = 26.84^o$	cir.cone $\alpha = 31.80^o$	cir.cone $\alpha = 30^o$
-	-	cone: 2 hours cylinder: 6 hours	5 min	

(d) cylinder and cone in Figure 3.b

AD	AED	SR	GF	true surface
ell.cylinder $r_{max} = 14.46$ $r_{min} = 13.51$	ell.cylinder $r_{max} = 14.64$ $r_{min} = 14.01$	cir.cylinder $r = 14.98$	cir.cylinder $r = 14.95$	cir.cylinder $r = 15.00$
sphere r=15.03	sphere r=15.05	sphere 15.03	sphere 14.95	sphere 15.00
-	-	sphere: 20 min cylinder: 2 hours	4 min	

(e) cylinder and sphere in Figure 3.c

Table 1: The tables list the results of the four algorithms on the main quadric surfaces in the test objects as well as the true answers. The computation time are shown in the last rows.

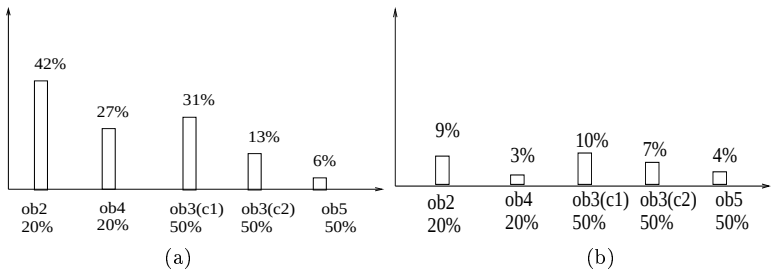

Figure 5: shape bias in the cylinder estimates (ob:object, c1:cylinder1,etc.). (a) with the AD technique, (b) with the AED technique

quadric surface, the estimate is greatly improved. When a specific algebraic function is used for the sphere (16) all the techniques give accurate estimates (Table 1(e)).

The computation time is dramatically high with the SR technique, and may take hours for surfaces with large amounts of data. This is normal with this non-linear representation where the data terms cannot be grouped and accumulated separately . Indeed the minimization criterion $J = \sum_{i=1}^{N} d(X_i, S)^2$ and its derivatives have to be computed sequentially by evaluating $d(X_i, S)^2$ at each point, thus the computation time gets higher as the number of points increases, whereas in the GF approach, the criterion $J = \vec{p}^T \mathcal{H} \vec{p}$ and its derivatives have the measurement points data encapsulated in the matrix $\mathcal{H}$ which is computed off-line, almost instantaneously. The GF technique has therefore very reasonable processing time (on the order of few minutes) for all the objects.

Although it is not the objective of this work we believe that using all the known relationships between the quadric surfaces and other surfaces very likely shifts the position of the surfaces towards their actual positions in the sense that incorporating these constraints may compensate for the effects of systematic errors. This aspect was mentioned in [9] for the circularity of the quadric. Generalizing this aspect for geometric relationships between surfaces can be worthwhile future work.

The optimization technique used in the GF algorithms supposes a reasonable initialisation of the surface parameter vector. Although this condition limits the field of application of the technique, it is well satisfied in our framework. We propose to use the estimates given by the AD, or, when possible, the AED as initialization. More generally we suggest the scheme illustrated in Figure 6 for optimal combination of the AD, AED and the GF for the estimation of object surfaces.

Acknowledgements

The work presented in this paper was funded by UK EPSRC grant GR /L25110. A short version of the paper has been published in the International Conference on Recent advances in 3-D Digital Imaging and Modeling, Ottawa, Canada.

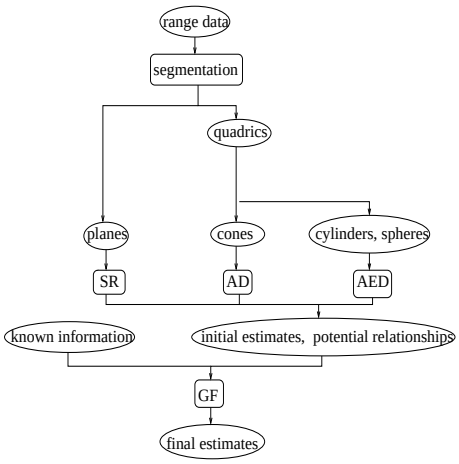

Figure 6: General scheme for object surfaces estimation.

References

1. O.D.Faugeras, M. Hebert, The Representation, Recognition and Positioning of 3-D Shapes from Range Data, *in Techniques for 3-D Machine Perception, ed. A. Rosenfeld*, North-Holland, Amsterdam, 1986.
2. K.T.Gunnarsson, F.B. Prinz, CAD model-based localization of parts in manufacturing, *IEEE Comput.*, **20**, No.8, 66–74, Aug. 1987.
3. G. Taubin, Estimation of Planar Curves, Surfaces and Non-planar Space Curves Defined by Implicit Equations with Applications to Edge and Range Image Segmentation, *IEEE Trans. PAMI*, **13**, No.11, 1115–1138, November 1991.
4. S.Kumar, S.Han, D.Goldgof, K.Boyer, On Recovering Hyperquadrics from Range data, *IEEE Trans. PAMI*, **17**, No.11, 1079–1083, November 1995.
5. G.Taubin, An Improved Algorithm For Algebraic Curve and Surface Fitting, *Proc. ICCV'93*, Berlin, Germany, 658–665, May 1993
6. G. Lukacs, A.D. Marshall and R.R. Martin. Faithful least-squares fitting of spheres, cylinders, cones and tori for reliable segmentation, *Proc. ECCV'98*, **1**, 671–686, Friburg, Germany, June 1998.
7. Z.Lei, D.B Cooper, Linear Programming Fitting of Implicit Polynomials, *IEEE Trans. PAMI*, **20**, No.2, 212–217, February 1998.
8. S.Sullivan, L.Sandford, J.Ponce, Using Geometric Distance Fits for 3-D object Modelling and Recognition, *IEEE Trans. PAMI*, **16**, No.12, 1183–1196, December 1994.
9. R.M.Bolle, D.B.Cooper, On Optimally Combining Pieces of Information, with Application to Estimating 3-D Complex-Object Position from Range Data, *IEEE Trans. PAMI* **8**, No.5, 619–638, September 1986.
10. P.J.Flynn, A.K.Jain, Surface Classification: Hypothesizing and Parameter Estimation, *Proc. IEEE Comp. Soc. CVPR*, 261–267. June 1988.
11. N. Werghi, R.B. Fisher, A. Ashbrook, C.Robertson, Object reconstruction by incorporating geometric constraints in reverse engineering, *Computer-Aided Design*, **31**, No.6, 363–399, May 1999.
12. A. Hoover, G. Jean-Baptiste, X. Jiang, P. J. Flynn, H. Bunke, D. Goldgof, K. Bowyer, D. Eggert, A. Fitzgibbon, R. Fisher, An Experimental Comparison of Range Segmentation Algorithms, *IEEE Trans. PAMI*, **18**, No.7, 673–689, July 1996.

Appendix

A first order approximation [3] of the Euclidean distance squared between a measurement point X and its projection $\hat{X}$ on the fitted surface is:

$$(X-\hat{X})^T(X-\hat{X}) \simeq \frac{f(\vec{p},X)^2}{\|\vec{\nabla} f(\vec{p},X)\|^2} \tag{20}$$

We consider the Euclidean distance weighted by the variances of measurement noise:

$$(X-\hat{X})^T L^{-1}(X-\hat{X}) \tag{21}$$

where L^{-1} is the covariance matrix of the measurement points defined by

$$L = \begin{bmatrix} \sigma_x^2 & 0 & 0 \\ 0 & \sigma_y^2 & 0 \\ 0 & 0 & \sigma_z^2 \end{bmatrix}$$

The values of the variances deduced from empirical tests are $\sigma_x = 0.05mm$, $\sigma_y = 0.05mm$ and $\sigma_z = 0.1mm$. These variances are related to the measurement errors of the measurement point coordinates. They are independent of the object size.

By considering $L^{-1} = R^T R$, (21) becomes $(RX - R\hat{X})^T(RX - R\hat{X})$ Thus from (20) we get

$$(X-\hat{X})^T L^{-1}(X-\hat{X}) \simeq \frac{f(\vec{p},RX)^2}{\|\vec{\nabla} f(\vec{p},RX)\|^2}$$

since

$$\frac{\partial f(\vec{p},RX)}{\partial RX} = R^T \frac{\partial f(\vec{p},RX)}{\partial X}$$

(21) could be expressed as

$$\begin{aligned} (X-\hat{X})^T L^{-1}(X-\hat{X}) &\simeq \frac{f(\vec{p},RX)^2}{(\frac{\partial f(\vec{p},RX)}{\partial X})^T R^T R (\frac{\partial f(\vec{p},RX)}{\partial X})} \\ &= \frac{f(\vec{p},RX)^2}{(\frac{\partial f(\vec{p},RX)}{\partial X})^T L^{-1} (\frac{\partial f(\vec{p},RX)}{\partial X})} \end{aligned}$$